PNAS RESEARCH ARTICLE | CELL BIOLOGY

An intact pituitary vasopressin system is critical for building a robust circadian clock in the suprachiasmatic nucleus

Yoshiaki Yamaguchi[a,b,1], Yota Maekawa[a], Kyohei Kabashima[a], Takanobu Mizuno[a], Motomi Tainaka[a], Toru Suzuki[a], Kumiko Dojo[a], Takeichiro Tominaga[a], Sayaka Kuroiwa[a], Satoru Masubuchi[c], Masao Doi[a], Keiko Tominaga[d], Kazuto Kobayashi[e], Satoshi Yamagata[f], Keiichi Itoi[f,g], Manabu Abe[h,i], William J. Schwartz[j], Kenji Sakimura[h,i], and Hitoshi Okamura[a,k,1]

Edited by Joseph Takahashi, The University of Texas Southwestern Medical Center, Dallas, TX; received May 22, 2023; accepted September 12, 2023

The circadian clock is a biological timekeeping system that oscillates with a circa-24-h period, reset by environmental timing cues, especially light, to the 24-h day–night cycle. In mammals, a "central" clock in the hypothalamic suprachiasmatic nucleus (SCN) synchronizes "peripheral" clocks throughout the body to regulate behavior, metabolism, and physiology. A key feature of the clock's oscillation is resistance to abrupt perturbations, but the mechanisms underlying such robustness are not well understood. Here, we probe clock robustness to unexpected photic perturbation by measuring the speed of reentrainment of the murine locomotor rhythm after an abrupt advance of the light–dark cycle. Using an intersectional genetic approach, we implicate a critical role for arginine vasopressin pathways, both central within the SCN and peripheral from the anterior pituitary.

circadian clock | suprachiasmatic nucleus | vasopressin | pituitary

Virtually, all organisms have an internal timekeeping system, which oscillates with an endogenous "free-running" period of close to 24 h ("circa-dian") that can be accurately synchronized (entrained) to exactly 24 h by daily environmental timing cues, especially light (1–3). In mammals, the master circadian clock in the suprachiasmatic nucleus (SCN) of the hypothalamus governs peripheral clocks throughout the brain and the body for temporal control of cellular metabolism and physiology. To function as a reliable "clock", the SCN must measure time with cycle-to-cycle precision; that is, its rhythm must be *robust* in the face of errant variations or random perturbations that might interfere with its sustained oscillation.

A "jet lag" protocol is a useful, noninvasive, quantifiable, behavioral assessment of the capacity of the SCN to resist a shift in its ongoing oscillation after a sudden large shift in the timing of the external light–dark (LD) cycle; its robustness against this perturbation may be gauged by measuring the rate at which the locomotor activity rhythms of experimental animals resynchronize after a sudden 8-h advance or delay of the LD cycle. Resetting of the behavioral rhythm is not completed immediately but proceeds slowly over several days; in C57BL/6 inbred mice, it takes approximately 10 d for complete reentrainment when the LD cycle is advanced by 8 h (4). A less robust, compromised system, with less capacity to withstand the external shift, would be expected to reentrain more quickly, in fewer days.

Most research on the mechanisms underlying the robustness of the circadian system has focused on the SCN, both at the intracellular molecular level and at the intercellular network level (5–7). We have previously reported that mice globally deficient in arginine vasopressin (AVP) receptors V1a and V1b ($V1a^{-/-}V1b^{-/-}$ mice) exhibit essentially immediate, complete shifts in circadian rhythms of behavior, body temperature, and gene expression in response to an abruptly shifted LD cycle, suggesting that these receptors are critical for the robustness of the circadian clock to this perturbation (4).

Here, we systematically elucidate the basis for AVP signaling in providing circadian robustness using an intersectional genetic approach. Our results reveal crucial roles for an unexpected extra-SCN source involving the anterior pituitary and for an intra-SCN source involving the neuropeptide somatostatin.

Results

AVP and V1a in the SCN Partially Contribute to Conferring Circadian Robustness. We first sought to determine the role of intrinsic SCN AVP signaling by generating three SCN-specific lines of knockout mice. First, we generated SCN-specific *AVP* knockout ($SCN\text{-}AVP^{-/-}$) mice by crossing *AVP*-floxed mice, in which exon 1 of the *AVP* gene is loxP-flanked (floxed), with *SCN-Cre* mice that have Cre recombinase (Cre) expression

Significance

While researchers have elucidated mechanisms underlying the circadian clock's innate oscillation and its light responsiveness, the molecular and cellular machinery responsible for its resistance to incidental perturbations remains uncertain. We studied the central mammalian clock in the suprachiasmatic nucleus (SCN) and the role of the neuropeptide arginine vasopressin (AVP), recognized as a major neurotransmitter in SCN neurons and for coherent SCN output. Using a variety of conditional knockout mouse lines, we show that robustness of this master clock is mediated by two independent AVP pathways, one inside the SCN via AVP-V1a receptors and the other outside the SCN via anterior pituitary AVP-V1b receptors. Even though the SCN can function as an autonomous clock, its resilience depends on extra-SCN tissue feedback.

Author contributions: Y.Y. and H.O. designed research; Y.Y., Y.M., K. Kabashima, T.M., M.T., T.S., K.D., T.T., S.K., S.M., M.D., and K.T. performed research; Y.Y., K. Kobayashi, S.Y., K.I., M.A., and K.S. contributed new reagents/analytic tools; Y.Y. analyzed data; and Y.Y., W.J.S., and H.O. wrote the paper.

The authors declare no competing interest.

This article is a PNAS Direct Submission.

[1]To whom correspondence may be addressed. Email: yama@kansai-u.ac.jp or okamura.hitoshi.4u@kyoto-u.ac.jp.

This article contains supporting information online at https://www.pnas.org/lookup/suppl/doi:10.1073/pnas.2308489120/-/DCSupplemental.

Published October 16, 2023.

directed to inhibitory GABAergic neurons under the control of the *Vgat* promoter (*SI Appendix*, Fig. S1 *A* and *B*) (8), since AVP neurons in the SCN are GABAergic, whereas those in the paraventricular nucleus (PVN) and the supraoptic nucleus (SON) are not (9–11). Indeed, immunohistochemical analyses revealed that AVP expression was totally disrupted in the SCN of the mutant mice (*SI Appendix*, Fig. S1*C*), while expression in the PVN, SON, and the median eminence (ME) was not affected (*SI Appendix*, Fig. S1 *D*–*F*). Although AVP depletion in the SCN did not cause overt gross abnormalities, lethality, or infertility, we and other researchers (12) have found that global AVP deficiency causes death at or shortly after birth. We note that AVP cells outside the SCN would also be affected if the cells were GABAergic.

Second, SCN-specific *V1a* knockout (*SCN-V1a*$^{-/-}$) mice were generated by crossing *V1a*-floxed mice, in which the coding region in exon 2 of the *V1a* gene is loxP-flanked (*SI Appendix*, Fig. S2 *A* and *B*), with *SCN-Cre* mice. V1a is expressed not only in the SCN but also in other tissues or organs, such as the liver (13). qPCR-based measurements revealed that *V1a* expression was completely abolished in the SCN of *SCN-V1a*$^{-/-}$ mice but not in the liver (*SI Appendix*, Fig. S2*C*). This was in contrast to liver-specific *V1a* knockout (*Alb-V1a*$^{-/-}$) mice, generated by crossing *V1a*-floxed mice with *Albumin-Cre* mice that express Cre driven by the *albumin* promoter, a reliable hepatocyte-specific promoter (14); as expected, *V1a* expression was completely lost in the liver of *Alb-V1a*$^{-/-}$ mice, but not in the SCN (*SI Appendix*, Fig. S2*C*). We confirmed that global *V1a* knockout (*V1a*$^{-/-}$) mice, generated by using *CAG-Cre* mice that express Cre under the control of the ubiquitous CAG promoter, did not express *V1a* in either SCN or liver (*SI Appendix*, Fig. S2*C*).

Third, since *V1b* has been reported to be expressed in the SCN by in situ hybridization (15, 16), we generated SCN-specific *V1b* knockout (*SCN-V1b*$^{-/-}$) mice by crossing *V1b*-floxed mice, in which the coding region in exon 2 of the *V1b* gene is loxP-flanked (*SI Appendix*, Fig. S3 *A* and *B*), with *SCN-Cre* mice.

By using these mutant mice, we examined the effect(s) of SCN-specific deletion of *AVP*, *V1a*, or *V1b* on the regulation of the speed of reentrainment after the LD cycle was abruptly advanced by 8 h (Fig. 1 *A* and *B*). To quantitatively compare reentrainment speeds measured in mice of each genotype, we calculated 50% phase-shift values (PS_{50}) (17). Compared to wild-type (WT) mice, *SCN-AVP*$^{-/-}$ and *SCN-V1a*$^{-/-}$ mice exhibited a significantly faster reentrainment to the shifted LD cycle (PS_{50} of ~6.1, ~4.3, and ~4.0 d, for WT, *SCN-AVP*$^{-/-}$, and *SCN-V1a*$^{-/-}$, respectively, Fig. 1*C*). In contrast, although global *V1b* knockout (*V1b*$^{-/-}$) mice, generated by mating with *CAG-Cre* mice, also reentrained significantly faster (PS_{50} of ~3.8 d), *SCN-V1b*$^{-/-}$ mice showed a similar speed of reentrainment to WT as well as to *AVP*$^{flox/flox}$, *V1a*$^{flox/flox}$, *Alb-V1a*$^{-/-}$, *V1b*$^{flox/flox}$, *SCN-Cre*, and *Alb-Cre* mice (Fig. 1*C* and *SI Appendix*, Fig. S4), suggesting that AVP and V1a within the SCN and V1b outside the SCN have roles in reentrainment kinetics under jet lag. Of note, the period length of locomotor activity

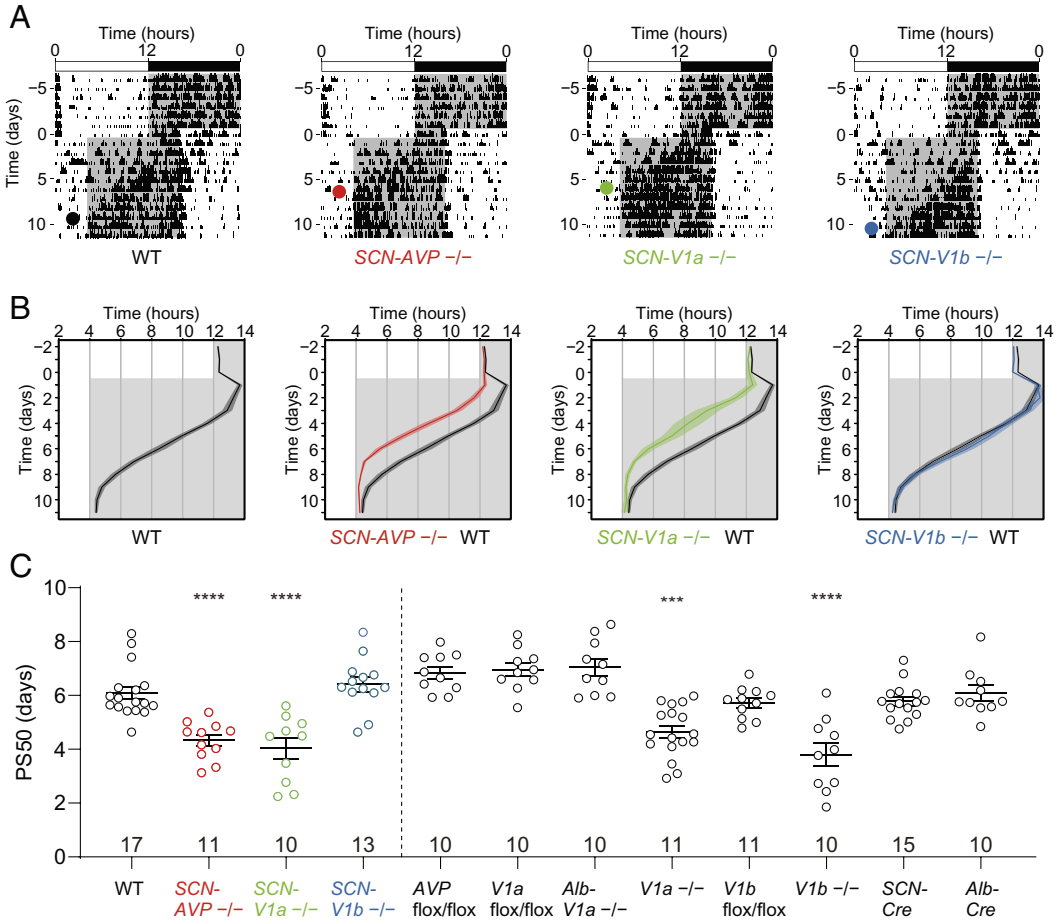

Fig. 1. *SCN-AVP*$^{-/-}$ and *SCN-V1a*$^{-/-}$ mice, but not *SCN-V1b*$^{-/-}$ mice, show faster reentrainment after LD advance. (*A*) Representative single-plotted actograms of WT, *SCN-AVP*$^{-/-}$, *SCN-V1a*$^{-/-}$, and *SCN-V1b*$^{-/-}$ mice subjected to an 8-h phase advance of the LD cycle. Black, red, and green-filled circles indicate assessed day of completed phase advance of activity onset. (*B*) Activity onset in the 8-h phase advance [means ± SEM; *n* = 17 (WT), 11 (*SCN-AVP*$^{-/-}$), 10 (*SCN-V1a*$^{-/-}$), and 13 (*SCN-V1b*$^{-/-}$)]. The data of WT mice are replicated for reference. (*C*) PS_{50} values in phase advance (means ± SEM; *n* for groups as shown; ****$P < 0.0001$, ***$P < 0.001$, one-way ANOVA with Dunnett post hoc test).

rhythms in constant darkness (DD), the phase angle from LD to DD, and the magnitude of phase shift after a short light pulse in *SCN-AVP*$^{-/-}$ and *SCN-V1a*$^{-/-}$ mice were essentially identical to those in WT mice (*SI Appendix*, Fig. S5), excluding the interpretation that rapid reentrainment in *SCN-AVP*$^{-/-}$ and *SCN-V1a*$^{-/-}$ mice was simply caused by an impaired clock, an advanced clock, or increased light sensitivity.

We considered the possibility that *V1b* had not been efficiently disrupted in the SCN of *SCN-V1b*$^{-/-}$ mice; however, using qPCR-based measurements, we found instead that *V1b* was not expressed in WT SCN samples obtained by laser-microdissection technique (*SI Appendix*, Fig. S6*A*), in contrast to the well-known circadian expression of *Per2* (*SI Appendix*, Fig. S6*B*) or *V1a* (*SI Appendix*, Fig. S6*C*) in the same SCN samples. The lack of detectable *V1b* expression in the SCN is thus consistent with our genetic data showing that *SCN-V1b*$^{-/-}$ mice reentrain to the shifted LD cycle with a speed similar to that of WT, in contrast to the rapid reentrainment of *V1b*$^{-/-}$ mice. Based on these results, we reasoned that V1b outside the SCN must play a critical role in the *V1b*$^{-/-}$ circadian phenotype, and to implicate candidate locations, we systematically checked *V1b* expression sites by qPCR using tissue/organ-specific samples. Using the same primers targeting *V1b*, we were able to successfully detect *V1b* expression in the pituitary (*SI Appendix*, Fig. S6*A*), where *V1b* mRNA has been reported to be abundantly expressed (18–20).

V1b in the Pituitary and AVP in CRF (Corticotropin-Releasing Factor) Neurons Are Involved in the Speed of Reentrainment. We next characterized a daily *V1b* expression profile using pituitary samples collected at 4-h intervals over 24 h. *V1b* expression in the pituitary showed no rhythmicity but was consistently high throughout the day (*SI Appendix*, Fig. S6*D*). Interestingly, we found exclusive expression of *V1b* in the pituitary, with no expression of *V1a* (*SI Appendix*, Fig. S6*C*) or *V2* (*SI Appendix*, Fig. S6*E*), suggesting that *V1a*, *V1b*, and *V2*, are expressed in the SCN, pituitary, and kidney, respectively. Since the pituitary gland is composed of three lobes (anterior, intermediate, and posterior), each with unique functions, we further investigated which parts of the pituitary gland express *V1b* using a laser-microdissection technique (*SI Appendix*, Fig. S6*E*). We found that *V1b* was expressed in the anterior pituitary, but we could not detect *V1b* in either the posterior or intermediate lobe (*SI Appendix*, Fig. S6 *F* and *G*).

The pituitary gland itself has been tested previously as a potential site of the master circadian clock. However, based on extensive studies in rats, Richter concluded that the pituitary gland, like other endocrine glands, is not essential for the generation of circadian locomotor activity rhythms (21). Indeed, researchers found that, in contrast to SCN lesions (22, 23), hypophysectomy (HPX) did not abolish rhythmicity (24–26). However, a role for the pituitary gland in setting reentrainment speed under jet-lag conditions has not been reported. We found that when we abruptly advanced the LD cycle by 8 h, HPX mice reentrained to the new cycle significantly faster than non-HPX mice (Fig. 2 *A*–*C*); the HPX PS_{50} value of ~4.0 d, similar to that of *V1b*$^{-/-}$ mice (PS_{50} ~3.8 d), suggests that V1b in the anterior pituitary contributes to regulating the speed of reentrainment under jet lag. Behavioral analyses confirmed that the period length of locomotor activity rhythms in DD, the phase angle from LD to DD, and the magnitude of phase shift after a short light pulse in HPX mice were essentially identical to those in non-HPX mice (*SI Appendix*, Fig. S7).

V1b-expressing cells in the anterior pituitary receive AVP secreted by parvocellular neurons of the PVN projecting to the external zone of the ME and transported via the pituitary portal vein. These parvocellular AVP neurons, which are distinct from AVP neurons in the magnocellular PVN and SON that release AVP from the posterior pituitary as an antidiuretic hormone, coexpress CRF and synergistically stimulate adrenocorticotropic hormone (ACTH)-releasing cells in the anterior pituitary (27, 28) (Fig. 2*D*).

Since *V1b* is exclusively expressed in the ACTH cells in the anterior pituitary (29), we utilized Cre driven by the promoter of proopiomelanocortin (*Pomc*), the precursor of ACTH (30), to specifically knockout *V1b* in the anterior pituitary. In Pomc-positive cell-specific *V1b* conditional knockout (*Pomc-V1b*$^{-/-}$) mice, generated by mating *Pomc-Cre* mice with *V1b*$^{flox/flox}$ mice, *V1b* expression was specifically and completely deleted in the pituitary but was not affected in the hippocampus, a site of high *V1b* expression (31), (*SI Appendix*, Fig. S3*C*). Expectedly, *Pomc-V1b*$^{-/-}$ mice exhibited significantly faster reentrainment than WT mice when the LD cycle was advanced by 8 h, with a reentrainment speed comparable to that of global *V1b*$^{-/-}$ and HPX mice (PS_{50} of ~6.1, ~3.4, ~3.8, and ~4.0 d for WT, *Pomc-V1b*$^{-/-}$, *V1b*$^{-/-}$, and HPX, respectively, Fig. 2 *C*, *E*, *F*, and *I*). Reentrainment speed of *V1b*$^{flox/flox}$ and *Pomc-Cre* mice was not significantly different from that of WT mice (Figs. 1*C* and 2*I*). To further examine the role of the parvocellular PVN AVP/CRF neurons that act on the V1b-expressing ACTH cells, we generated CRF-positive cell-specific *AVP* conditional knockout (*CRF-AVP*$^{-/-}$) mice by mating *CRF-Cre* mice with *AVP*$^{flox/flox}$ mice. In *CRF-AVP*$^{-/-}$ mice, AVP immunoreactivity in the external zone of the ME, the terminals of CRF neurons, was significantly decreased compared to control *AVP*$^{flox/flox}$ and *CRF-Cre* mice, whereas AVP in the internal zone was not changed (*SI Appendix*, Fig. S8), indicating that AVP was selectively down-regulated in parvocellular AVP/CRF neurons but not in magnocellular neurons. We found that *CRF-AVP*$^{-/-}$ mice showed significantly faster reentrainment after an 8-h LD cycle advance than WT mice (Fig. 2 *G*–*I*), indicating that AVP in CRF neurons is involved in the modulation of reentrainment speed under jet lag. Behavioral analyses confirmed that the period length of locomotor activity rhythms in DD, the phase angle from LD to DD, and the magnitude of phase shift after a short light pulse in *Pomc-V1b*$^{-/-}$ and *CRF-AVP*$^{-/-}$ mice were essentially identical to those in WT mice (*SI Appendix*, Fig. S5).

SCN-V1a$^{-/-}$; Pomc-V1b$^{-/-}$ Double Conditional Knockout Mice Exhibit Immediate Reentrainment. Our data above demonstrate that V1a in the SCN and V1b in the Pomc cells regulate reentrainment speed under jet lag. If these two receptors function independently, double-mutant mice should reentrain even faster than either single-mutant mice alone. Indeed, *SCN-V1a*$^{-/-}$; *Pomc-V1b*$^{-/-}$ double conditional knockout (*SCN-V1a*$^{-/-}$; *Pomc-V1b*$^{-/-}$) mice exhibited essentially immediate, complete reentrainment compared to WT, *SCN-V1a*$^{-/-}$, and *Pomc-V1b*$^{-/-}$ mice after the 8-h advance of the LD cycle (PS_{50} of ~6.1, ~4.0, ~3.4, and ~1.4 d for WT,*SCN-V1a*$^{-/-}$, *Pomc-V1b*$^{-/-}$, and *SCN-V1a*$^{-/-}$; *Pomc-V1b*$^{-/-}$, respectively, Fig. 3). The immediate re-entrainment phenotype of *SCN-V1a*$^{-/-}$; *Pomc-V1b*$^{-/-}$ mice thus can reproduce that of the global *V1a*$^{-/-}$; *V1b*$^{-/-}$ mice that we had previously reported (4). Of note, *SCN-V1a*$^{-/-}$; *Pomc-V1b*$^{-/-}$ mice did not show any alteration in period length in DD, the phase angle from LD to DD, or the magnitude of phase shift after a short light pulse (*SI Appendix*, Fig. S5).

SCN Somatostatin Is Involved in the Speed of Reentrainment. How is the pituitary involved in the regulation of re-entrainment under jet lag? To determine the effect of pituitary ablation on the SCN clock, we examined gene expression profiles in the SCN of HPX mice (Fig. 4 *A* and *B*). A customized panel of 38 SCN

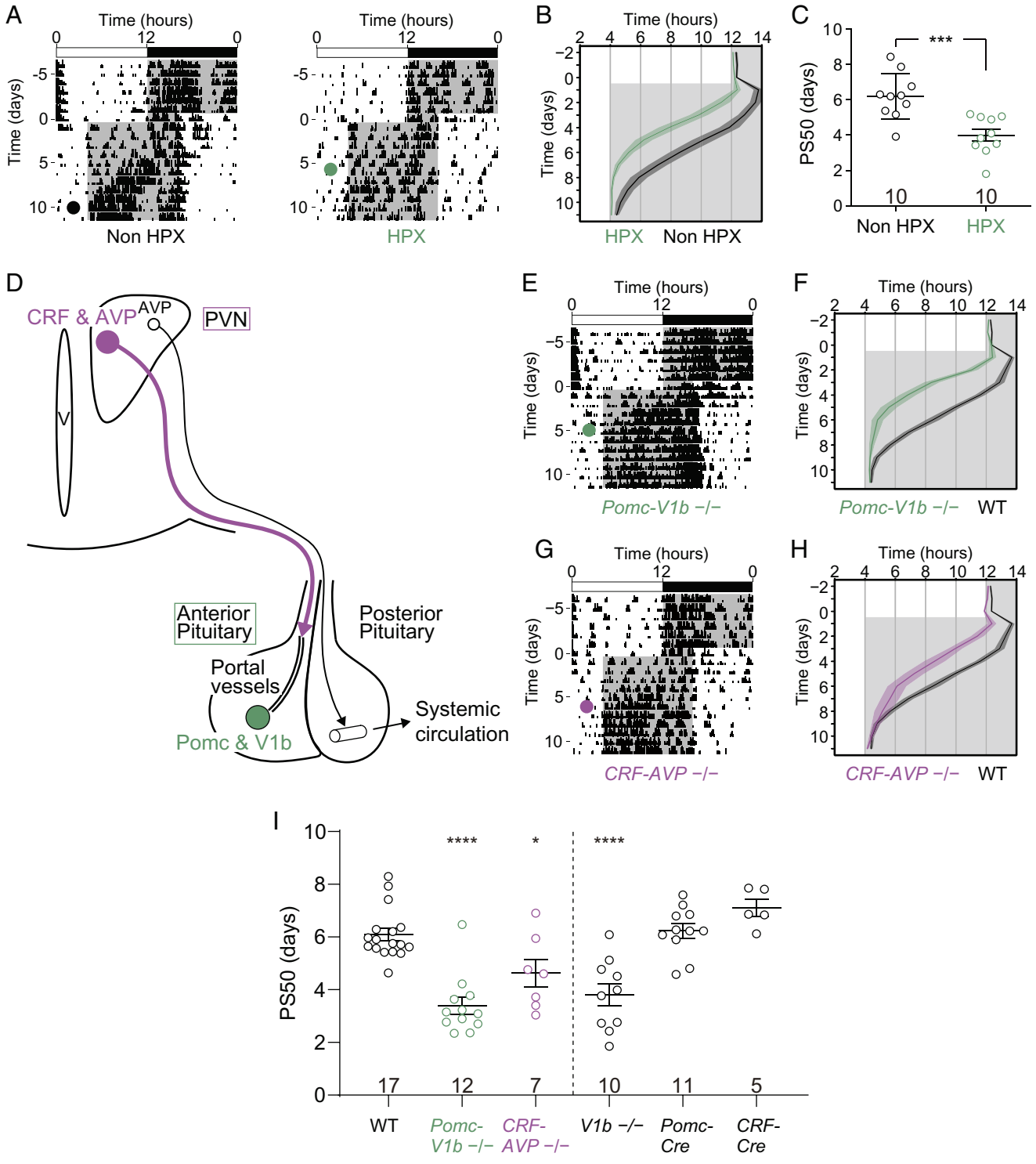

Fig. 2. HPX, *Pomc-V1b*$^{-/-}$, and *CRF-AVP*$^{-/-}$ mice show faster reentrainment after LD advance. (*A*) Representative single-plotted actograms of Non-HPX and HPX mice subjected to an 8-h phase advance of the LD cycle. Black and green-filled circles indicate assessed day of completed phase advance of activity onset. (*B*) Activity onset in the 8-h phase advance (means ± SEM; *n* = 10 for both Non-HPX and HPX mice). (*C*) PS_{50} values in phase advance (means ± SEM; *n* for groups as shown; ***$P < 0.001$, unpaired *t* test). (*D*) Schematic diagram showing AVP released from CRF neurons in the PVN is delivered to Pomc-positive V1b expressing neurons in the anterior pituitary. (*E*) Representative single-plotted actogram of a *Pomc-V1b*$^{-/-}$ mouse subjected to an 8-h phase advance of the LD cycle. Green-filled circle indicates assessed day of completed phase advance of activity onset. (*F*) Activity onset in the 8-h phase advance (means ± SEM; *n* = 12 for *Pomc-V1b*$^{-/-}$ mice). The data of WT mice are replicated for reference. (*G*) Representative single-plotted actogram of a *CRF-AVP*$^{-/-}$ mouse subjected to an 8-h phase advance of the LD cycle. Magenta-filled circle indicates assessed day of completed phase advance of activity onset. (*H*) Activity onset in the 8-h phase advance (means ± SEM; *n* = 7 for *CRF-AVP*$^{-/-}$ mice). The data of WT mice are replicated for reference. (*I*) PS_{50} values in phase advance (means ± SEM; *n* for groups as shown; ****$P < 0.0001$, *$P < 0.05$, one-way ANOVA with Dunnett post hoc test). The data of WT and *V1b*$^{-/-}$ mice are replicated for reference.

genes, including representative core clock genes, clock-controlled genes, and circadian clock-related neurotransmitters and receptors, was analyzed by quantitative RT-PCR using the Fluidigm system (32, 33). Measurement at 6 time points before and after an 8-h advance of the LD cycle revealed preferentially and consistently downregulated mRNA expression of *somatostatin* (*SST*) in the SCN of HPX mice compared to control non-HPX mice, while other genes remained unaltered (Fig. 4*B*). The reduction in *SST*

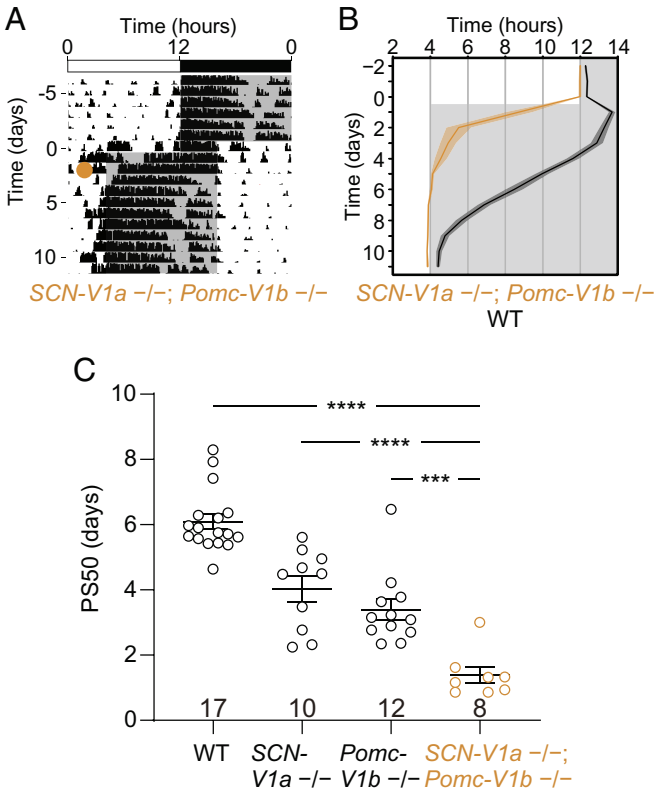

Fig. 3. Double conditional *SCN-V1a*$^{-/-}$; *Pomc-V1b*$^{-/-}$ mice reentrained faster than *SCN-V1a*$^{-/-}$ or *Pomc-V1b*$^{-/-}$ mice after LD advance. (*A*) Representative single-plotted actogram of a *SCN-V1a*$^{-/-}$; *Pomc-V1b*$^{-/-}$ mouse subjected to an 8-h phase advance of the LD cycle. Orange-filled circle indicates assessed day of completed phase advance of activity onset. (*B*) Activity onset in the 8-h phase advance (means ± SEM; *n* = 8 for *SCN-V1a*$^{-/-}$; *Pomc-V1b*$^{-/-}$ mice). The data of WT mice are replicated for reference. (*C*) PS_{50} values in phase advance (means ± SEM; *n* for groups as shown; ****$P < 0.0001$, ***$P < 0.001$, one-way ANOVA with Dunnett post hoc test). The data of WT, *SCN-V1a*$^{-/-}$, and *Pomc-V1b*$^{-/-}$ mice are replicated for reference.

gene expression was further confirmed using the StepOnePlus Real-Time PCR system (Fig. 4*C*). Microarray analysis revealed that *SST* showed the strongest signal intensity among the genes whose expression levels were reduced by more than 1.7-fold in the SCN of HPX mice compared to non-HPX mice at both ZT2 and ZT14 (*SI Appendix*, Table S1).

SST has been implicated in circadian rhythmicity (34–36) and phase shifts (37, 38). We next performed SST immunohistochemistry in the SCN to examine whether reduced *SST* gene expression was reflected in SST protein expression and its histological distribution in HPX mice. As previously reported, SST neurons were located in the dorsomedial region and projected to the ventrolateral region of the SCN (39, 40), where SST receptor subtype 1 (SSTR1) is expressed (41). SSTR1 is the only SST receptor expressed in the SCN (*SI Appendix*, Fig. S9), although its circadian function remains unknown. In the SCN of HPX mice, SST axonal arborization was significantly reduced compared to that of non-HPX mice (Fig. 4*D*). A similar significant decrease in SST innervation was also observed in the SCN of *V1b*$^{-/-}$ and *Pomc-V1b*$^{-/-}$ mice, but not of *V1b*$^{flox/flox}$ or *V1a*$^{-/-}$ mice, compared to WT mice (Fig. 4*E*). These results indicate that pituitary V1b plays a pivotal role in maintaining SST innervation in the SCN.

To investigate whether SST affects reentrainment speed after the LD cycle advance, we generated *SST* mutant (*SST*$^{m/m}$) mice (*SI Appendix*, Fig. S10). *SST*$^{m/m}$ mice, deficient in *SST* mRNA and protein expression (*SI Appendix*, Fig. S10), as well as *SSTR1*$^{-/-}$ mice, exhibited significantly faster reentrainment after the advance than WT mice (Fig. 4 *F–H*), with PS_{50} values comparable to those for *CRF-AVP*$^{-/-}$ and *Pomc-V1b*$^{-/-}$ mice. During the preparation of our manuscript, other investigators also reported a similar phenotype of *SST*$^{-/-}$ mice (42). Behavioral analyses confirmed that the period length in DD, the phase angle from LD to DD, and the magnitude of phase shift after a short light pulse in *SST*$^{m/m}$ and *SSTR1*$^{-/-}$ mice were essentially identical to those in WT mice (*SI Appendix*, Fig. S5). These results indicate that SST-SSTR1 in the SCN, which is affected by pituitary V1b, plays an important role in the regulation of reentrainment speed under jet lag.

Discussion

To probe the robustness of the circadian clock's oscillation to an unexpected photic perturbation, we measured the speed of reentrainment of the murine locomotor activity rhythm after a sudden 8-h advance of the LD cycle. Using an intersectional genetic approach, we have demonstrated that the inactivation of two pathways—an intra-SCN AVP/V1a pathway and an extra-SCN V1b pathway from parvocellular PVN AVP/CRF neurons to anterior pituitary ACTH cells—dramatically diminishes circadian robustness, decreasing the PS_{50} from 6 d to little more than 1 d, with the V1b pathway presumably acting via regulation of SCN SST-SSTR1 activity. Importantly, *SCN-V1a*$^{-/-}$; *Pomc-V1b*$^{-/-}$ double conditional knockout mice exhibit essentially immediate, complete reentrainment compared to either *SCN-V1a*$^{-/-}$ or *Pomc-V1b*$^{-/-}$ mice alone, indicating the independent and additive contribution of the SCN AVP/V1a and PVN AVP/pituitary V1b pathways to the robustness of the clock (*SI Appendix*, Fig. S11).

AVP and CRF are coproduced in the parvocellular PVN (27, 43) and released into the pituitary portal vessels, where they act on V1b and CRF1 receptors, respectively, on corticotroph cells to stimulate ACTH release and activate the hypothalamic-pituitary-adrenal (HPA) axis (44). Glucocorticoids released from the adrenal cortex are known to modulate reentrainment under jet lag (17, 45). Taken together with our present findings, we conclude that the activity of an intact AVP/V1b-driven HPA axis plays a crucial role in building a robust circadian clock in vivo.

All life activities, including behavior, are based on homeostasis, in which physiological variables such as body temperature and fluid balance are maintained within a certain range. The hypothalamus and pituitary are the primary regulators of homeostasis, with the HPA axis playing a major role in controlling the response to stress and regulating many biological processes, including digestion, energy storage and expenditure, mood and emotion, and immune function. Our present results argue that "central" circadian clock function under the "stress" of jet lag is not exempt from "peripheral" modulation by the HPA axis via a PVN AVP/pituitary V1b mechanism.

Materials and Methods

Animals. *AVP-flox* mice were designed and generated by Keiichi Itoi, Kenji Sakimura, and their lab members to address a different experimental issue from the present study, which has been submitted elsewhere (46). To generate *AVP-flox*, *V1a-flox*, and *V1b-flox* mice, targeting vectors were designed in which exon 1 of the mouse *Avp* gene, amino acids coding region in exon 2 of the mouse *V1a* gene, and amino acids coding region in exon 2 of the mouse *V1b* gene, respectively, were flanked by two loxP sites. Each targeting vector was constructed with C57BL/6 genomic fragments containing 6.5 kb 5′ arm and 5.3 kb 3′ arm (*Avp-flox*), 5.4 kb 5′ arm and 5.8 kb 3′ arm (*V1a-flox*), and 5.2 kb 5′ arm and 5.9 kb 3′ arm (*V1b-flox*), a neomycin resistance cassette, and a diphtheria toxin gene. The linearized targeting vector was electroporated into the C57BL/6 embryonic stem cell line RENKA (47). Correctly targeted clones were identified by Southern blotting using 5′, 3′, and neo probes. The ES cells evaluated to have the correct

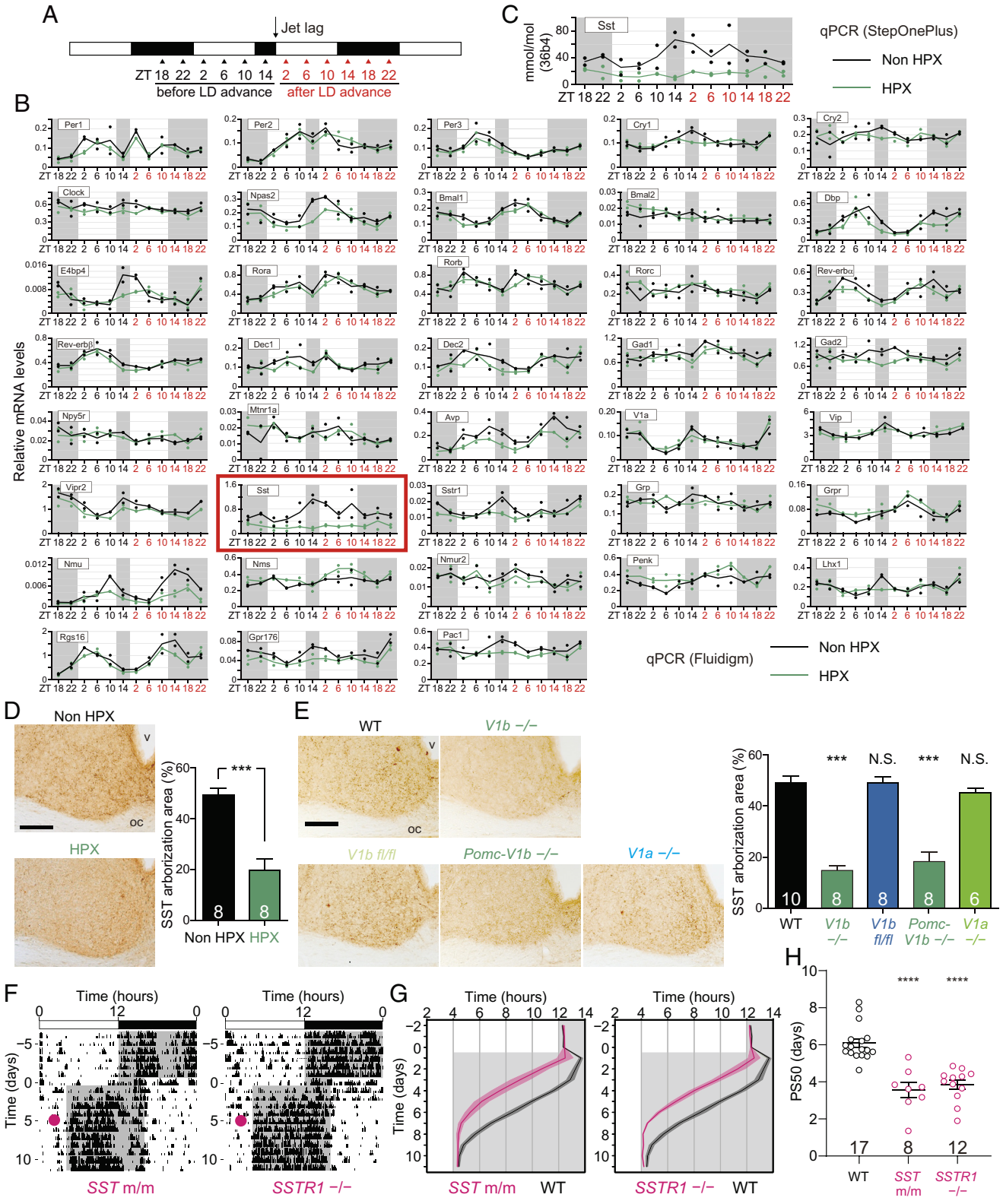

Fig. 4. *SST*$^{m/m}$ and *SSTR1*$^{-/-}$ mice show faster reentrainment after LD advance. (*A*) Sampling time course before and after LD advance. Triangles indicate the sampling time points, with black and red indicating before and after LD advance, respectively. (*B*) mRNA expression profiles of representative core clock genes, clock-controlled genes, circadian clock-related neurotransmitters and receptors in the SCN of Non-HPX (black) and HPX (green) mice, with *Sst* expression profiles highlighted within a red frame. Graph indicates an average of two mice independently collected and measured. (*C*) *Sst* mRNA expression was measured with StepOnePlus and normalized against *36b4* mRNA. (*D*) Representative images of SST immunoreactivity in the SCN of Non-HPX and HPX mice. (Scale bar, 100 μm); oc, optic chiasm; v, third ventricle. SST arborization areas are also shown (means ± SEM; $n = 8$ for both Non-HPX and HPX mice; ***$P < 0.001$, unpaired *t* test). (*E*) Representative images of SST immunoreactivity in the SCN of WT, *V1b*$^{-/-}$*V1b*$^{flox/flox}$*Pomc-V1b*$^{-/-}$, and *V1a*$^{-/-}$ mice. (Scale bar, 100 μm); oc, optic chiasm; v, third ventricle. SST arborization areas are also shown (means ± SEM; *n* for groups as shown; ***$P < 0.001$, one-way ANOVA with Dunnett post hoc test). (*F*) Representative single-plotted actograms of *SST*$^{m/m}$ and *SSTR1*$^{-/-}$ mice subjected to an 8-h phase advance of the LD cycle. Red-filled circles indicate assessed day of completed phase advance of activity onset. (*G*) Activity onset in the 8-h phase advance [means ± SEM; $n = 8$ (*SST*$^{m/m}$) and 12 (*SSTR1*$^{-/-}$)]. The data of WT mice are replicated for reference. (*H*) PS_{50} values in phase advance (means ± SEM; *n* for groups as shown; ****$P < 0.0001$, one-way ANOVA with Dunnett post hoc test). The data of WT mice are replicated for reference.

recombination were used to yield chimeric mice as described previously (48). Chimeric mice were mated with C57BL/6 mice, and the offspring were further crossed with Flippase expressing B6-Tg(CAG-FLPe)37 mice (RIKEN BRC Stock No: RBRC01835) to yield floxed heterozygous mice (49). Global knockout mice were generated by mating with B6.Cg-Tg(CAG-Cre)CZ-MO2Osb mice (RIKEN BRC Stock No: RBRC01828) (50). To generate SCN-, liver-, pituitary-, and CRF cells-specific knockout mice, each of the floxed mice was crossed with Slc32a1$^{tm2(cre)Lowl}$/J mice (The Jackson Lab. Stock No: 016962), Albumin-Cre mice (51), Tg(Pomc1-cre)16Lowl/J mice (The Jackson Lab. Stock No: 005965), and CRF-Cre mice (52), respectively. These Cre recombinase-expressing mice were backcrossed into the C57BL/6 background for at least 8 generations before mating with floxed mice. All the Cre genotypes used in this study were heterozygous. Mutant mice for the gene encoding *SST* were generated by gene targeting with mouse ES cells as described previously (53). The targeting vector contained the 5′-homologous region of 8.5 kb of the *SST* gene, the internal ribosomal entry site, the cDNA encoding human interleukin-2 receptor α-subunit (IL-2Rα) fused to green fluorescent protein, the phosphoglycerate kinase-1 promoter-neo resistant gene cassette (*PGK-neo*) flanked by the two loxP sites, the 3′-homologous region of 2.6 kb of the *SST* gene, and the diphtheria toxin A-fragment gene cassette (*SI Appendix*, Fig. S10). Mice heterozygous for the targeted mutation (*SST*$^{+/neo}$) were bred with Cre transgenic mice to delete the *PGK-neo* gene cassette. Resultant heterozygous mutant mice (*SST*$^{+/m}$) were backcrossed with C57BL/6J mice for more than 9 generations and used to obtain homozygous mutant mice (*SST*$^{m/m}$). *SST*$^{m/m}$ mice develop normally without somatic gigantism, as reported in a line of *SST*$^{-/-}$ mice (54). *SSTR1*$^{-/-}$ mice were generated as described previously (55), and backcrossed into the C57BL/6 background. HPX mice were purchased from Shimizu Laboratory Supplies (Kyoto, Japan). Mice (2 to 5 mo old, age-matched between genotypes) were used for immunohistochemistry or gene expression analysis.

Behavioral Activity Monitoring for Jet-Lag Experiments. Mice (2 to 3 mo old, age-matched between genotypes) were individually housed in light-tight, ventilated closets in a temperature- and humidity-controlled facility with ad libitum access to food and water. The animals were entrained to a 12-h-light (~200 lx fluorescent light)/12-h-dark (LD) cycle for at least ten days to synchronize (entrain) the circadian clock to the ambient LD cycle, and then, the LD cycles were phase-advanced by 8 h. Locomotor activity was recorded in 5-min bins with a passive (pyroelectric) infrared sensor (FA-05 F5B; Omron), and the data obtained were analyzed with ClockLab software (Actimetrics) developed on MatLab (Mathworks). To better assess the rate of reentrainment, in this study, we used the PS_{50} value obtained by calculating the daily onset times after LD advance, rather than a single data point when reentrainment was completed. Onset times of locomotor activities under jet lag were determined by careful observation of all activity data, using offset times and smooth behavioral transitions over several days as a reference whenever possible. To determine PS_{50} values, sigmoidal dose–response curves with variable slope, $Y = Bottom + (Top - Bottom)/(1 + 10^{(log\ PS50\ -\ X)\ HillSlope})$, were fitted to the onset time points of locomotor activity using GraphPad Prism software (17). The free-running period was determined by fitting a linear regression line to the activity onsets, based on animal behaviors over a 14-d interval taken 3 d after the start of the DD condition. The magnitude of phase shifts in behavioral activity after release to DD was determined as the time difference between the regression lines of activity onsets before and after the start of DD. For the light pulse-induced phase-shift experiments, mice put in DD were exposed to a light pulse for 30 min at CT14. The amplitude of light-induced phase shifts is greatest at CT14, which is appropriate for the comparison of light responsiveness between genotypes. Phase shifts were quantified as the time difference before and after the light application. All experiments were conducted in accordance with the ethical guidelines of the Kyoto University Animal Research Committee.

Immunohistochemistry. For immunohistochemistry of AVP and SST, animals were anesthetized and perfused with cold fixative (4% paraformaldehyde in 0.1 M PB) at ZT4. After fixation, coronal brain sections (30 μm thick) cut on a cryostat microtome (CM3050S, Leica) were processed for free-floating immunohistochemistry with rabbit polyclonal antibody against AVP (Merck, AB1565, 1:5,000 dilution) and rabbit polyclonal antibody against SST (Peninsula Laboratories International, T-4103, 1:5,000 dilution). The sections were then incubated with biotinylated anti-rabbit IgG (Vector Laboratories, BA-1000, 1:1,000 dilution). Immunoreactivities were visualized with a peroxidase-based Vectastain Elite ABC kit (Vector Laboratories) using diaminobenzidine chromogen. For quantitative analysis of SST axonal arborization areas in the SCN, micrographs obtained with a Carl Zeiss Axiovert 200 microscope and 20× objective lens were binarized using ImageJ, and an innervated area of each nucleus was obtained by averaging the areas of 5 sections containing the nucleus by a person blinded to the genotype of the mice.

Laser Microdissection of the SCN and the Pituitary. Mice were killed by cervical dislocation, and the eyes were removed under a red safety light when the samples were collected in the dark condition. The brain or the pituitary was then isolated from the skull under room light and immediately frozen on dry ice. Coronal brain or pituitary sections (30-μm thick) were prepared on a cryostat and mounted on POL-membrane slides (Leica) as described previously (4). Sections were fixed in an ice-cold mixture of ethanol and acetic acid, stained with 0.05% toluidine blue, and air dried quickly. Once the moisture in the sections decreased sufficiently for laser cutting, cells in the SCN or the pituitary were microdissected using an LMD7000 device (Leica; 10× magnification) and lysed in TRIzol reagent (Thermo Fisher Scientific), and total RNA was purified using the RNeasy micro kit (Qiagen).

Quantitative RT-PCR. Total RNA from the SCN, hippocampus, liver, pituitary, and kidney was converted to cDNA using the SuperScript VILO cDNA Synthesis Kit (Thermo Fisher Scientific). Quantitative PCR analysis of each cDNA was performed as previously described (56). Absolute quantification of each gene level was achieved by comparison to the cloned plasmid DNA as a standard, and results were normalized to *36b4* mRNA levels. Melt curve analysis was performed to confirm each final PCR product. Primer sequences are shown in *SI Appendix*, Table S2.

Fluidigm. qPCR was performed on a BioMark HD System using a 48.48 Fluidigm BioMark Dynamic Array chip (Fluidigm) (32). Data were normalized to *36b4*. Primer and probe sequences are shown in *SI Appendix*, Table S3.

Microarray Analysis. In order to identify changes in gene expression in the SCN of HPX mice, SCN tissue samples obtained by laser microdissection technique from 10 animals at ZT2 and 10 animals at ZT14 were pooled in TRIzol reagent (Thermo Fisher Scientific). Total RNA was isolated from the lysate using the RNeasy micro kit (Qiagen), and the integrity was assessed by analyzing aliquots on an Agilent 2100 Bioanalyzer (Agilent Technologies). Single-stranded cDNA synthesis and labeling were performed using GeneChip WT PLUS Reagent Kit (Affymetrix), and subsequent hybridization was performed with GeneChip Mouse Gene 2.0 ST Array (Affymetrix) according to the manufacturer's protocol. The data were analyzed with Affymetrix Expression Console (Affymetrix) using the RMA algorithm for normalization. For statistical analysis of the microarray data, we obtained values of 11 probes for the seminal proteins (Svs1, Svs2, Svs3a, Svs3b, Svs4, Svs5, Svs6, Sva, Sval1, Sval2, and Sval3) that were unlikely to be expressed in the SCN. We then subtracted the mean of 11 probes from the value of each gene assuming the mean value to represent zero expression. DNA microarray data have been deposited at GEO under accession number GSE226929.

In Situ Hybridization. In situ hybridization analysis was performed as described (57) using the following gene-specific probes: for *SSTR1*, the anti-sense probe covering nucleotides 57 to 620 of the *SSTR1* mRNA (Genbank, NM_009216), for *SSTR2* (502 to 902, NM_009217), for *SSTR3* (824 to 1,051, NM_009218), for *SSTR4* (1,633 to 2,156, NM_009219), for *SSTR5* (419 to 650, MMU82697), and for *SST* (36 to 524, NM_009215).

Northern Blotting. Whole-brain RNA was extracted using TRIzol (Invitrogen). Northern blot analysis was performed as described previously (58). ^{32}P-radiolabeled probe for *SST* (36 to 524, NM_009215) was generated by RT-PCR.

Data, Materials, and Software Availability. DNA microarray data have been deposited in GEO (GSE226929) (59).

ACKNOWLEDGMENTS. We thank Dr. Paola Bagnoli for providing *SSTR1*$^{-/-}$ mice. This work was supported in part by the Ministry of Education, Culture, Sports, Science, and Technology of Japan: Grant-in-aid for Scientific Research A (18H04015, H.O.), Young Scientists A (15H05642, Y.Y.), Scientific Research C (22K06594, Y.Y.), Challenging Research (Pioneering) (22K18384, H.O.), Exploratory Challenging Research (20K20864, K.T.), Specially Promoted Research (18002016, H.O.), AdAMS (16H06276, K.S.), grants from Core Research for Evolutional Science and Technology, Japan Science and Technology Agency (CREST/JPMJCR14W3,

H.O.), Kobayashi International Scholarship Foundation and SRF (H.O.), Grants from Brain Research Institute Niigata University, and BRIDGE Fellowship BR220401 from the Japan Society for Promotion of Science (M.D. and W.J.S.).

Author affiliations: [a]Department of Systems Biology, Graduate School of Pharmaceutical Sciences, Kyoto University, Kyoto 606-8501, Japan; [b]Department of Life Science and Biotechnology, Faculty of Chemistry, Materials and Bioengineering, Kansai University, Suita 564-8680, Japan; [c]Department of Physiology, School of Medicine, Aichi Medical University, Nagakute 480-1195, Japan; [d]Graduate School of Frontier Biosciences, Osaka University, Suita 565-0871, Japan; [e]Department of Molecular Genetics, Institute of Biomedical Sciences, Fukushima Medical University School of Medicine, Fukushima 960-1295, Japan; [f]Graduate School of Information Sciences, Tohoku University, Sendai 980-0845, Japan; [g]Department of Nursing, Faculty of Health Sciences, Tohoku Fukushi University, Sendai 981-8522, Japan; [h]Department of Cellular Neurobiology, Brain Research Institute, Niigata University, Niigata 951-8585, Japan; [i]Department of Animal Model Development, Brain Research Institute, Niigata University, Niigata 951-8585, Japan; [j]Department of Neurology, Dell Medical School, The University of Texas at Austin, Austin, TX 78712; and [k]Department of Neuroscience, Graduate School of Medicine, Kyoto University, Kyoto 606-8501, Japan

1. J. S. Takahashi, Transcriptional architecture of the mammalian circadian clock. *Nat. Rev. Genet.* **18**, 164–179 (2017).
2. M. H. Hastings, N. J. Smyllie, A. P. Patton, Molecular-genetic manipulation of the suprachiasmatic nucleus circadian clock. *J. Mol. Biol.* **432**, 3639–3660 (2020).
3. A. Patke, M. W. Young, S. Axelrod, Molecular mechanisms and physiological importance of circadian rhythms. *Nat. Rev. Mol. Cell Biol.* **21**, 67–84 (2020).
4. Y. Yamaguchi *et al.*, Mice genetically deficient in vasopressin V1a and V1b receptors are resistant to jet lag. *Science* **342**, 85–90 (2013).
5. J. A. Mohawk, C. B. Green, J. S. Takahashi, Central and peripheral circadian clocks in mammals. *Annu. Rev. Neurosci.* **35**, 445–462 (2012).
6. E. D. Herzog, T. Hermanstyne, N. J. Smyllie, M. H. Hastings, Regulating the suprachiasmatic nucleus (SCN) circadian clockwork: Interplay between cell-autonomous and circuit-level mechanisms. *Cold Spring Harb. Perspect. Biol.* **9**, a027706 (2017).
7. M. H. Hastings, E. S. Maywood, M. Brancaccio, Generation of circadian rhythms in the suprachiasmatic nucleus. *Nat. Rev. Neurosci.* **19**, 453–469 (2018).
8. D. R. Weaver *et al.*, Functionally complete excision of conditional alleles in the mouse suprachiasmatic nucleus by Vgat-ires-Cre. *J. Biol. Rhythms* **33**, 179–191 (2018).
9. M. Tanaka, T. Matsuda, Y. Shigeyoshi, Y. Ibata, H. Okamura, Peptide expression in GABAergic neurons in rat suprachiasmatic nucleus in comparison with other forebrain structures: A double labeling in situ hybridization study. *J. Histochem. Cytochem.* **45**, 1231–1237 (1997).
10. H. Okamura *et al.*, Demonstration of GABAergic cell bodies in the suprachiasmatic nucleus: In situ hybridization of glutamic acid decarboxylase (GAD) mRNA and immunocytochemistry of GAD and GABA. *Neurosci. Lett.* **102**, 131–136 (1989).
11. R. Y. Moore, J. C. Speh, GABA is the principal neurotransmitter of the circadian system. *Neurosci. Lett.* **150**, 112–116 (1993).
12. T. Yoshikawa *et al.*, Spatiotemporal profiles of arginine vasopressin transcription in cultured suprachiasmatic nucleus. *Eur. J. Neurosci.* **42**, 2678–2689 (2015).
13. A. Morel, A. M. O'Carroll, M. J. Brownstein, S. J. Lolait, Molecular cloning and expression of a rat V1a arginine vasopressin receptor. *Nature* **356**, 523–526 (1992).
14. C. Postic *et al.*, Dual roles for glucokinase in glucose homeostasis as determined by liver and pancreatic beta cell-specific gene knock-outs using Cre recombinase. *J. Biol. Chem.* **274**, 305–315 (1999).
15. T. Kalamatianos, I. Kallo, C. W. Coen, Ageing and the diurnal expression of the mRNAs for vasopressin and for the V1a and V1b vasopressin receptors in the suprachiasmatic nucleus of male rats. *J. Neuroendocrinol.* **16**, 493–501 (2004).
16. C. Vaccari, S. J. Lolait, N. L. Ostrowski, Comparative distribution of vasopressin V1b and oxytocin receptor messenger ribonucleic acids in brain. *Endocrinology* **139**, 5015–5033 (1998).
17. S. Kiessling, G. Eichele, H. Oster, Adrenal glucocorticoids have a key role in circadian resynchronization in a mouse model of jet lag. *J. Clin. Invest.* **120**, 2600–2609 (2010).
18. T. Sugimoto *et al.*, Molecular cloning and functional expression of a cDNA encoding the human V1b vasopressin receptor. *J. Biol. Chem.* **269**, 27088–27092 (1994).
19. S. J. Lolait *et al.*, Extrapituitary expression of the rat V1b vasopressin receptor gene. *Proc. Natl. Acad. Sci. U.S.A.* **92**, 6783–6787 (1995).
20. A. Tanoue *et al.*, The vasopressin V1b receptor critically regulates hypothalamic-pituitary-adrenal axis activity under both stress and resting conditions. *J. Clin. Invest.* **113**, 302–309 (2004).
21. C. P. Richter, *Biological Clocks in Medicine and Psychiatry* (Charles C. Thomas, 1965), pp. 1–110.
22. F. K. Stephan, I. Zucker, Circadian rhythms in drinking behavior and locomotor activity of rats are eliminated by hypothalamic lesions. *Proc. Natl. Acad. Sci. U.S.A.* **69**, 1583–1586 (1972).
23. R. Y. Moore, V. B. Eichler, Loss of a circadian adrenal corticosterone rhythm following suprachiasmatic lesions in the rat. *Brain Res.* **42**, 201–206 (1972).
24. D. J. Ferguson, M. B. Visscher, F. Halberg, L. M. Levy, Effects of hypophysectomy on daily temperature variation in C3H mice. *Am. J. Physiol.* **190**, 235–238 (1957).
25. M. Müller, H. Giersberg, Über den Einfluss der inneren Sekretion auf die tagesperiodische Aktivität der weissen Maus. *Z. Vgl. Physiol.* **40**, 454–472 (1957).
26. F. K. Stephan, I. Zucker, Rat drinking rhythms: Central visual pathways and endocrine factors mediating responsiveness to environmental illumination. *Physiol. Behav.* **8**, 315–326 (1972).
27. F. A. Antoni, Vasopressinergic control of pituitary adrenocorticotropin secretion comes of age. *Front. Neuroendocrinol.* **14**, 76–122 (1993).
28. J. C. Buckingham, The influence of vasopressin on hypothalamic corticotrophin releasing activity in rats with inherited diabetes insipidus. *J. Physiol.* **312**, 9–16 (1981).
29. F. Hernando, O. Schoots, S. J. Lolait, J. P. Burbach, Immunohistochemical localization of the vasopressin V1b receptor in the rat brain and pituitary gland: Anatomical support for its involvement in the central effects of vasopressin. *Endocrinology* **142**, 1659–1668 (2001).
30. N. Balthasar *et al.*, Leptin receptor signaling in POMC neurons is required for normal body weight homeostasis. *Neuron* **42**, 983–991 (2004).
31. W. S. Young, J. Li, S. R. Wersinger, M. Palkovits, The vasopressin 1b receptor is prominent in the hippocampal area CA2 where it is unaffected by restraint stress or adrenalectomy. *Neuroscience* **143**, 1031–1039 (2006).
32. J. M. Fustin *et al.*, RNA-methylation-dependent RNA processing controls the speed of the circadian clock. *Cell* **155**, 793–806 (2013).
33. M. Doi *et al.*, Non-coding cis-element of Period2 is essential for maintaining organismal circadian behaviour and body temperature rhythmicity. *Nat. Commun.* **10**, 2563 (2019).
34. J. Takeuchi, H. Nagasaki, K. Shinohara, S.-I.T. Inouye, A circadian rhythm of somatostatin messenger RNA levels, but not of vasoactive intestinal polypeptide/peptide histidine isoleucine messenger RNA levels in rat suprachiasmatic nucleus. *Mol. Cell. Neurosci.* **3**, 29–35 (1992).
35. J. Yang *et al.*, Day-night variation of preprosomatostatin messenger RNA level in the suprachiasmatic nucleus. *Mol. Cell. Neurosci.* **5**, 97–102 (1994).
36. T. Nishiwaki *et al.*, Differences of somatostatin mRNA in the rat suprachiasmatic nucleus under light-dark and constant dark conditions: An analysis by in situ hybridization. *Neurosci. Lett.* **197**, 231–234 (1995).
37. T. Hamada, S. Shibata, A. Tsuneyoshi, K. Tominaga, S. Watanabe, Effect of somatostatin on circadian rhythms of firing and 2-deoxyglucose uptake in rat suprachiasmatic slices. *Am. J. Physiol.* **265**, R1199–R1204 (1993).
38. C. Fukuhara *et al.*, Phase advances of circadian rhythms in somatostatin depleted rats: Effects of cysteamine on rhythms of locomotor activity and electrical discharge of the suprachiasmatic nucleus. *J. Comp. Physiol. A* **175**, 677–685 (1994).
39. M. Tanaka *et al.*, Somatostatin neurons form a distinct peptidergic neuronal group in the rat suprachiasmatic nucleus: A double labeling in situ hybridization study. *Neurosci. Lett.* **215**, 119–122 (1996).
40. S. Daikoku, S. Hisano, Y. Kagotani, Neuronal associations in the rat suprachiasmatic nucleus demonstrated by immunoelectron microscopy. *J. Comp. Neurol.* **325**, 559–571 (1992).
41. C. D. Breder *et al.*, Differential expression of somatostatin receptor subtypes in brain. *J. Neurosci.* **12**, 3920–3934 (1992).
42. D. A. M. Joye *et al.*, Somatostatin regulates central clock function and circadian responses to light. *Proc. Natl. Acad. Sci. U.S.A.* **120**, e2216820120 (2023).
43. P. E. Sawchenko, L. W. Swanson, W. W. Vale, Co-expression of corticotropin-releasing factor and vasopressin immunoreactivity in parvocellular neurosecretory neurons of the adrenalectomized rat. *Proc. Natl. Acad. Sci. U.S.A.* **81**, 1883–1887 (1984).
44. G. Aguilera, S. Subburaju, S. Young, J. Chen, The parvocellular vasopressinergic system and responsiveness of the hypothalamic pituitary adrenal axis during chronic stress. *Prog. Brain Res.* **170**, 29–39 (2008).
45. D. Sage *et al.*, Influence of the corticosterone rhythm on photic entrainment of locomotor activity in rats. *J. Biol. Rhythms* **19**, 144–156 (2004).
46. S. Yamagata *et al.*, Vasopressin expressed in hypothalamic CRF neurons causes impaired water diuresis in secondary adrenal insufficiency. *Endocrinology* **164**, bqad109 (2023), 10.1210/endocr/bqad109.
47. M. Mishina, K. Sakimura, Conditional gene targeting on the pure C57BL/6 genetic background. *Neurosci. Res.* **58**, 105–112 (2007).
48. M. Fukaya *et al.*, Abundant distribution of TARP gamma-8 in synaptic and extrasynaptic surface of hippocampal neurons and its major role in AMPA receptor expression on spines and dendrites. *Eur. J. Neurosci.* **24**, 2177–2190 (2006).
49. H. Kanki, H. Suzuki, S. Itohara, High-efficiency CAG-FLPe deleter mice in C57BL/6J background. *Exp. Anim.* **55**, 137–141 (2006).
50. H. Matsumura, H. Hasuwa, N. Inoue, M. Ikawa, M. Okabe, Lineage-specific cell disruption in living mice by Cre-mediated expression of diphtheria toxin A chain. *Biochem. Biophys. Res. Commun.* **321**, 275–279 (2004).
51. S. Shimba *et al.*, Deficient of a clock gene, brain and muscle Arnt-like protein-1 (BMAL1), induces dyslipidemia and ectopic fat formation. *PLoS One* **6**, e25231 (2011).
52. K. Itoi *et al.*, Visualization of corticotropin-releasing factor neurons by fluorescent proteins in the mouse brain and characterization of labeled neurons in the paraventricular nucleus of the hypothalamus. *Endocrinology* **155**, 4054–4060 (2014).
53. K. Kobayashi *et al.*, Targeted disruption of the tyrosine hydroxylase locus results in severe catecholamine depletion and perinatal lethality in mice. *J. Biol. Chem.* **270**, 27235–27243 (1995).
54. M. J. Low *et al.*, Somatostatin is required for masculinization of growth hormone-regulated hepatic gene expression but not of somatic growth. *J. Clin. Invest.* **107**, 1571–1580 (2001).
55. H. J. Kreienkamp, E. Akgun, H. Baumeister, W. Meyerhof, D. Richter, Somatostatin receptor subtype 1 modulates basal inhibition of growth hormone release in somatotrophs. *FEBS Lett.* **462**, 464–466 (1999).
56. M. Doi *et al.*, Salt-sensitive hypertension in circadian clock-deficient Cry-null mice involves dysregulated adrenal Hsd3b6. *Nat. Med.* **16**, 67–74 (2010).
57. Y. Shigeyoshi *et al.*, Light-induced resetting of a mammalian circadian clock is associated with rapid induction of the mPer1 transcript. *Cell* **91**, 1043–1053 (1997).
58. A. Ishida *et al.*, Light activates the adrenal gland: Timing of gene expression and glucocorticoid release. *Cell Metab.* **2**, 297–307 (2005).
59. Y. Yamaguchi, H. Okamura, Transcriptome profiling of circadian day and night gene expression in the suprachiasmatic nucleus of hypophysectomized (HPX) and control (non-HPX) mice. Gene Expression Omnibus. https://www.ncbi.nlm.nih.gov/geo/query/acc.cgi?acc=GSE226929. Deposited 8 March 2023.